Available online at www.sciencedirect.com

ScienceDirect

journal homepage: www.elsevier.com/locate/he

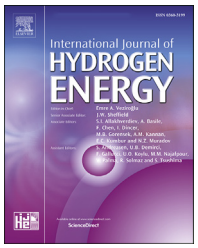

Decomposition studies of NH_3 and ND_3 in presence of H_2 and D_2 with Pt/Al_2O_3 and Ru/Al_2O_3 catalysts

Rodrigo Antunes [a,*], *Roland Steiner* [a], *Laurent Marot* [a], *Ernst Meyer* [a]

[a] *Department of Physics, University of Basel, Klingebergstrasse 82, CH-4056, Basel, Switzerland*

HIGHLIGHTS

- Decomposition efficiencies above 90% were obtained with NH_3 and ND_3 using Ru/Al_2O_3.
- The inhibition effect of H_2 and D_2 with Pt/Al_2O_3 was stronger than with Ru/Al_2O_3.
- NH_2D is the most important isotopologue in NH_3-D_2 and ND_3-H_2 mixtures.
- Ru/Al_2O_3 is the most suitable to be employed in the ITER Tokamak Exhaust Process.

ARTICLE INFO

Article history:
Received 18 October 2021
Received in revised form
17 February 2022
Accepted 18 February 2022
Available online 10 March 2022

Keywords:
Ammonia
Isotope
Decomposition
Platinum
Ruthenium

ABSTRACT

In the fusion reactor ITER, ammonia will be produced as a result of the interaction between the hydrogen isotopes used as fuel and nitrogen used to spread the power loads of a larger area. As part of the fuel management in ITER, NQ_3 (NQ_3, Q = H, D, T) will have to be decomposed using a palladium membrane reactor. The decomposition of pure NH_3 and ND_3 was studied in this work using commercial platinum (Pt) and ruthenium (Ru) catalysts on alumina (0.5 wt% loading), in a conventional reactor configuration (i.e., without a palladium membrane). With Pt/Al_2O_3, decomposition fractions larger than 90% were achieved with NH_3 above 800 K using the lowest flow-to-mass ratio (F_{NH_3}/g-cat) of 0.015 sccm g^{-1}. However, with the increase of F_{NH_3}/g-cat to 0.220 sccm g^{-1}, similar decompositions were achieved only at ≈1000 K. In contrast, with Ru/Al_2O_3 decomposition fractions above 90% were attained already below 700 K, regardless of F_{NH_3}/g-cat. With both catalysts the decomposition of NH_3 was found to be more efficient than that of ND_3 at a wide range of temperatures, thus evidencing the existence of isotopic effect. A strong inhibition of both NH_3 and ND_3 in presence of, respectively, H_2 and D_2 with Pt/Al_2O_3 was observed. This effect was stronger at lower temperatures and larger hydrogen partial pressures. The inhibition effect with Ru/Al_2O_3 was less pronounced and it was suppressed at 629 K. Isotopic exchange reactions with equimolar mixtures of NH_3-D_2 and ND_3-H_2 revealed that the most and least abundant isotopologue are, respectively, NH_2D and ND_3. At the relevant temperature window in which the PMR will be operated (673–823 K), the Ru-based catalyst exhibits superior performances in terms of decomposition rates, negligible isotopic and inhibition effects. A slight reduction of the performances with this catalyst was observed with 0.200 sccm g^{-1}. This work suggests that 0.5 wt% Ru/Al_2O_3 is the most suitable catalyst to be used during ITER operation.

* *Corresponiding author*.
E-mail address: rodrigo.antunes@unibas.ch (R. Antunes).

https://doi.org/10.1016/j.ijhydene.2022.02.155

Introduction

The decomposition of ammonia (NH_3) has attracted over the last two decades a great deal of attention for the potential use of NH_3 for hydrogen generation and storage [1–4]. Ruthenium is one of the most studied materials in the literature of ammonia decomposition because it exhibits the highest catalytic activity of all pure metals [5]. Several works have focused on the study of ruthenium-based catalysts with various support and promoters. Yin et al. reported a comprehensive study on Ru-supported catalysts, which included supports of carbon nanotubes (CNTs), titania (TiO_2), alumina (Al_2O_3) and activated carbon [6]. They reported superior catalytic activities for the CNT-based samples, with which NH_3 decomposition fractions above 80% were attained at 700 K using potassium as promoter. In contrast, similar NH_3 decompositions were obtained with Ru/Al_2O_3 only at 823 K. The larger performances for Ru/CNTs were attributed to a high amount of Ru surface atoms (i.e., high dispersion), to its high graphitization (leading to an easier electron transfer to ruthenium) and high purity of the CNTs. Other works with Al_2O_3-supported Ru catalysts showed that the decomposition rate of NH_3 was optimal with 2.2 nm wide Ru clusters [7]. Hill and Torrente-Murciano reported the enhancing effect of cesium (Cs) promoters on the activity of Ru/CNT [8]. With 7 wt% Ru 4 wt% Cs/graphitized CNT, NH_3 decomposition rates of 90% were achieved with temperatures as low as 600 K. Cs acts as a strong electron donor on the Ru surface and CNT support. With concentrations beyond 20 wt% the effect of Cs is however detrimental since it starts covering Ru active sites, thus hindering the adsorption of ammonia. Another class of catalysts studied for ammonia decomposition include metal nitrides and carbides. The enhanced catalytic activity of tungsten-carbide (WC) for various reactions was reported in the early 1970s [9]. The surface electronic properties of WC were found to be similar to that of Pt, thus explaining their similar activities. More recently, Zheng et al. showed that the catalytic activity of molybdenum carbide (Mo_2C) is comparable with that of 2 wt% Ru-graphite, which suggests the former to be a good candidate to replace catalysts based on noble metals [18]. The carbon and nitrogen atoms in the metal carbides and nitrides are located in the interstitial sites between the larger host atoms, thus altering the electronic properties of the surface and reducing the activation energy for ammonia decomposition [10]. Metal amides and imides have also been employed to catalyse the decomposition of ammonia. Two main examples are the decomposition over sodium amide ($NaNH_2$(s)) and lithium imide ($LiNH_2$(s)). With these materials, the reaction mechanisms are quite different from those discussed previously: the catalyst itself is cyclically altered over the course of the reaction. Lithium imide-amide has superior performances for ammonia decomposition when compared to ruthenium and nickel-based catalysts, achieving almost full decomposition at 773 K [11].

This paper is devoted to study the decomposition of ammonia using catalysts relevant for ITER, which is the next largest experimental nuclear fusion device, currently under construction in Cadarache, France. This reactor will be operated with deuterium (D) and tritium (T) [12]. Due to the large power loads foreseen at the so-called divertor region, nitrogen-seeding will be used to radiatively spread the power loads over larger areas [13]. The dissociation of molecular nitrogen in a hydrogen isotope plasma will unavoidably lead to the formation of NQ_3, where Q = H, D, T [14–17]. Ammonia will be trapped inside the cryopumps installed at the outlet of the ITER reactor, and it will be recovered by stagewise heating of the cryotraps. During this process, other molecules (e.g., Q_2, Q_2O, N_2, NQ_3) are expected to be desorbed as well. These species will be afterwards processed by the so-called Tokamak Exhaust Processing (TEP) system. The first stage of TEP consists of palladium membrane reactors (PMRs), which combine palladium (or palladium-based) membranes and catalysts [18,19]. The catalyst installed in the feed side of the reactor, operated between 673 and 823 K, will promote the cracking of Q-containing molecules. For instance, NQ_3 will be decomposed through the endothermic reaction $NQ_3 \rightarrow 1.5\ Q_2 + 0.5\ N_2$. Consequently, the Q_2 molecules present in the feed stream will permeate through the Pd membrane, thanks to its exclusive selectivity towards Q_2. While it is currently not known neither the composition of the gas mixture nor the gas flow feeding the PMRs, the desired efficiency for ammonia decomposition is >99%.

The choice of the catalyst for ITER purposes is constrained by the use of the radioactive tritium. For instance, promising catalysts such as those supported on CNTs are undesirable since carbon-based supports in combination with metals, hydrogen and high temperature can undergo methanation, which can impose serious pushbacks for practical purposes [5,20]. Also, the catalysts should not themselves be a potential tritium sink. This would be the case of imide-amide catalysts, which consist of hydrogen atoms and since the reaction steps involve cyclic transformative steps between the catalyst and the gas phase, isotopic exchanges will unavoidably occur between the flowing gas (for instance, ND_3) and the hydrogen atoms of the catalyst [11,21,22]. Consequently, the use of these materials at the outlet of the ITER vacuum vessel would lead to an increase in fuel retention, which must be minimized.

Based on the readiness level and material relevancy, commercial platinum- and ruthenium-based catalysts have been selected for the purpose of ammonia decomposition in view of ITER. In this work, the decomposition efficiencies of NH_3 and ND_3 using platinum and ruthenium on alumina pellets (with 0.5 wt% loading) are compared over a wide range of relevant conditions, i.e. temperature, Q_2 and N_2 inlet concentrations and flow-to-mass ratios. The use of NH_3 and ND_3 allow studying the existence of isotopic effect on their conversion to Q_2. Moreover, since the composition and flow of the gas feeding the PMR are currently not known, we further investigate the influence of the flow-to-catalyst-mass ratios and the impact of the Q_2 and N_2 concentrations on the ammonia decomposition. The presence of H_2 has been reported to hinder the decomposition of NH_3 on Pt and Ru [7, 23], which could be detrimental for the recovery of the hydrogen isotopes in ITER. The likely presence of mixed isotopologues (e.g., DT-ND_3) in the feed side of the PMR will lead to the formation of heavier ammonia isotopologues, which could further influence the efficiency of ammonia decomposition. Thus, the results obtained through isotopic exchange reactions occurring between flowing mixtures of NH_3-D_2 and ND_3-H_2 are also discussed.

Experimental

Selected catalysts and experimental matrix

Two catalysts from Sigma-Aldrich were selected for this work: Pt and Ru supported on Al_2O_3, with an active surface concentration of 0.5 wt%. Both catalysts feature a 3.2 mm pellet shape and a porosity width distribution with the most frequent value (mode) of 8.145 nm. The BET surface area of Pt/Al_2O_3 was found to be around 106.7 $m^2\ g^{-1}$, which is slightly higher than that of Ru/Al_2O_3 (99.1 $m^2\ g^{-1}$).

The experimental matrix displayed in Table 1 was defined based on the foreseen set of conditions to be used with the PMR deployed at the UKAEA, which aims at demonstrating the ITER TEP process [19]. This PMR has been commissioned with 180 g of Pt/Al_2O_3 and it is planned to process ammonia-containing flows in the range of 10–100 sccm (standard cubic centimeter per minute). These conditions correspond to total flow-to-mass ratios F_t/g-cat of 0.05–0.55 sccm g^{-1}. While the ammonia concentration in these streams should be as high as possible, for safety reasons NH_3 cannot be handled in pure form at UKAEA and it will be diluted down to 10% in argon. Thus, the ratio between the flow of NH_3 and mass of catalyst (F_{NH_3}/g-cat) will be actually shifted to 0.005 to 0.055 sccm g^{-1}. In our work, we used pure ammonia and studied F_{NQ_3}/g-cat ratios between 0.01 and 0.22 sccm g^{-1}. Note that the larger flow-to-mass values allow investigating scenarios where large amounts of ammonia would be released during stagewise heating of the cryotraps. The ratio between the ammonia flow and the catalyst mass was varied by changing the latter from around 0.8 to roughly 12 g, while keeping $F_{NQ_3} \approx 0.18$ sccm. Three flow-to-mass ratios are discussed in this work and will be referred to as $F^L \approx 0.015$ sccm g^{-1} (low), $F^M \approx 0.058$ sccm g^{-1} (medium), $F^{H,1} \approx 0.200$ sccm g^{-1} and $F^{H,2} \approx 0.220$ sccm g^{-1} (high).

All experiments were carried out at constant ammonia flows of $F_{NQ_3} \approx 0.18$ sccm, equivalent to partial pressures of 1.5 Pa. The temperature dependency experiments were carried out from 300 to 927 K. The inhibition effect of H_2 and D_2 on the decomposition of NH_3 and ND_3 was studied by simultaneously feeding the reactor with mixtures of NH_3–H_2 and ND_3-D_2. The flow of Q_2 was varied to reach concentrations up to 50 mol%, yielding a total pressure of ≈3 Pa. Similar experiments were done to investigate the role of N_2 up to 58 mol% (total pressure of ≈3.5 Pa). The isotopic exchange reaction studies were done with equimolar mixtures of NH_3-D_2 and ND_3-H_2 at 3 Pa and up to 927 K.

Experimental setup and procedure

The schematic diagram of the experimental setup is presented in Fig. 1. It consists of a quartz tube (31 mm inner diameter and a length of 1400 mm), which connects the gas supply side to a high-vacuum chamber inside which a Residual Gas Analyser (RGA, Stanford Research Systems, SRS 200) is installed. Thanks to the PEEK pinhole (2 mm wide) placed at the end of the quartz tube, the pressures inside the quartz cylinder can be kept at a few Pa during experiments, whereas the RGA chamber is maintained at ~ 10^{-4} Pa. The catalyst is installed in the furnace zone (Nabertherm GmbH), that is used to impose the desired temperatures. The furnace features a three-zone heating, thus ensuring a homogeneous temperature along the catalyst region. The gases are injected either through a needle valve (NH_3, ND_3) or with mass-flow controllers (H_2, D_2, N_2), BrooksGF40. All gases are of high purity (99.9999%), except D_2 with 99.7%. The isotopic composition of ND_3 is of 99% D and 1% H. After introducing the catalyst inside the setup, the sample was activated by outgassing it overnight at 10^{-2} Pa and at elevated temperatures (up to 900 K), which led to the desorption of mainly H_2O, N_2 and CO_2. This process was found to be equivalent to outgassing the sample in presence of Ar (0.6 Pa) up to 673 K, followed by H_2 introduction (10% in Ar) for 2 h. In a typical experiment, pure NH_3 or ND_3 is injected with a partial pressure of 1.5 Pa (corresponding to flows of ≈0.18 sccm) with the oven set to a given temperature. The composition of the resulting gas mixture at the end of the quartz tube and the steady-state of the process are evaluated using the intensity of the relevant RGA peaks, which are continuously recorded. With this procedure, the decomposition rate DR can be determined by the relative difference between the ammonia concentration at the inlet ($NQ_{3,in}$) and its concentration at the outlet ($NQ_{3,out}$), given by Equation (1). Typical relative uncertainties obtained throughout this work lie in the range of 5–10%.

$$DR(\%) = 100 \times \frac{NQ_{3,in} - NQ_{3,out}}{NQ_{3,in}} \quad (1)$$

It is worth mentioning that, even without catalyst, thermal decomposition of NH_3 and ND_3 can be achieved with our quartz setup. However, the decomposition only starts at

Table 1 – Experimental matrix.

	0.5 wt% Pt/Al_2O_3		0.5 wt% Ru/Al_2O_3		
Installed mass (g)	12.4	0.8	12.0	3.1	0.9
Flow-to-mass (sccm g^{-1})	0.015 (F^L)	0.220 ($F^{H,2}$)	0.015 (F^L)	0.058 (F^M)	0.200 ($F^{H,1}$)
Pressure (Pa)	1.5–3.6 Pa		1.5–3.6 Pa	1.5 Pa	
Temperature (K)	300 – 927 K		300 – 710 K		
Ammonia decomposition	pure NH_3, pure ND_3		pure NH_3, pure ND_3	pure NH_3	
Hydrogen inhibition	up to 50 mol% H_2, D_2		up to 50 mol% H_2, D_2	–	
Nitrogen inhibition	up to 58 mol% N_2		up to 58 mol% N_2	–	
Isotopic exchange reactions	50-50 mol% NH_3-D_2		50-50 mol% NH_3-D_2	–	
	50-50 mol% ND_3-H_2		50-50 mol% NH_3-D_2	–	

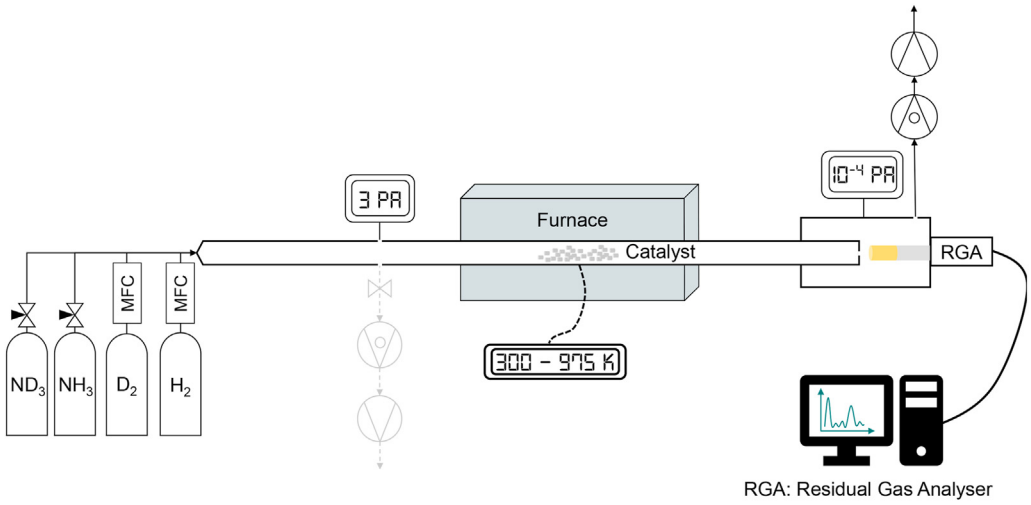

Fig. 1 – Schematic diagram of the experimental setup used for the ammonia decomposition and isotopic exchange experiments.

temperatures above 900 K, which, as discussed below, is negligible compared to the activity of both catalysts and therefore its contribution can be neglected.

Results and discussion

Effect of temperature

Fig. 2a shows the effect of temperature on the decomposition of NH_3 and ND_3 obtained with F^L and $F^{H,2}$ using Pt/Al_2O_3. Within the ITER-relevant temperature window (673–823 K), the decomposition of ammonia varies substantially. For instance, the DR of NH_3 with F^L increases from around 40% to slightly over 90% in this temperature range. The decomposition of both NH_3 and ND_3 is more efficient with F^L, which is explained by the larger active surface area available to decompose the same ammonia flow. For instance, at 757 K the NH_3 decomposition increases from 34 to 78% with the decrease of F_{NH_3}/g-cat. Also, at comparable temperatures and F_{NH_3}/g-cat ratios, the decomposition of NH_3 is found to be larger than that of ND_3, which evidences the existence of isotopic effect.

Fig. 2b) shows the decomposition of ammonia over Ru/Al_2O_3 for various temperatures. The most striking difference is the temperature range within which high conversion rates can be achieved. With Ru/Al_2O_3 decomposition fractions well above 90% are obtained within the ITER-relevant temperature window. The larger performances for ruthenium are explained by its superior activity for ammonia decomposition, which is the largest of all pure metals [24]. Moreover, the effect of the flow-to-mass ratio seems to be less critical with the ruthenium-based catalyst. Indeed, it is interesting to note that the performances obtained with $F^L \approx 0.015\,\mathrm{sccm\,g^{-1}}$ and $F^M \approx 0.058\,\mathrm{sccm\,g^{-1}}$ are quite similar. The arithmetic differences between the DRs shown in Fig. 2 were calculated to have a simple measure of the isotopic shift. These results are plotted in Fig. 3. The isotopic shift seems to be more

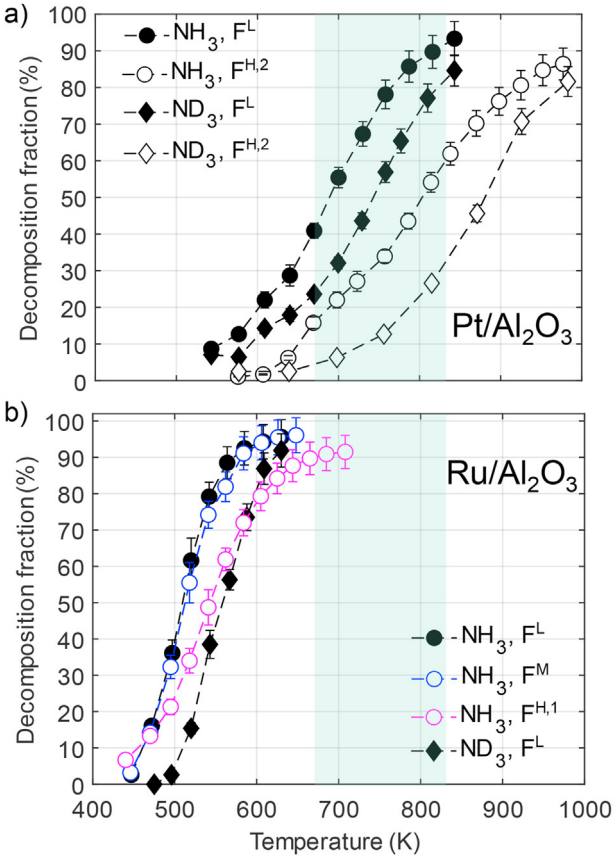

Fig. 2 – Decomposition of ammonia as a function of the catalyst temperature with a) Pt/Al_2O_3 and b) Ru/Al_2O_3. Circles: NH_3, diamonds: ND_3. For a), filled symbols: with F^L, empty symbols: with $F^{H,2}$. For b), filled symbols: with F^L, empty symbols: with $F^{H,1}$ (magenta) and F^M (blue). The range of temperatures foreseen for ITER operation is highlighted as well. (For interpretation of the references to color in this figure legend, the reader is referred to the Web version of this article.)

pronounced for Ru/Al_2O_3, with which the difference between the decomposition of NH_3 and ND_3 can be as high as 40% at 475 K. In contrast, this difference reaches a maximum between 20 and 30% for Pt/Al_2O_3 in the range between 720 and 810 K.

The isotopic effect on the decomposition of NH_3 and ND_3 is an indication that a surface reaction involving at least one scission of N-Q is rate-limiting [23]. The lower decomposition efficiencies for ND_3 when compared to NH_3 using platinum and ruthenium have been previously reported. Vajo et al. concluded that at 0.13 Pa the reaction rates for the decomposition of both molecules converge at low temperatures, below 500 K [23]. At higher temperatures (up to ≈1000 K), the decomposition of NH_3 was found to take place at a faster rate. However, at pressures above 27 Pa the Pt activity for NH_3 and ND_3 converged in the temperature range of interest. On ruthenium, the isotopic effect was studied by Egawa et al. in the range of 520–598 K at pressures below 10^{-3} Pa [25]. They concluded that until 541 K NH_3 decomposes more efficiently, while at higher temperatures both NH_3 and ND_3 decompose at similar rates. Interestingly, our results with Ru/Al_2O_3 evidence the existence of isotopic effect up to slightly higher temperatures (≈590K, as displayed in Fig. 3).

Effect of H_2, D_2 and N_2 partial pressures

During the stagewise heating of the cryotraps, it is expected that other species will be desorbed along with ammonia. Thus, we studied the influence of Q_2 and N_2 on the decomposition of ammonia. In these experiments, NH_3–H_2 and ND_3-D_2 mixtures with varying partial pressures of Q_2 were fed into the reactor. As shown in Fig. 4a, for F^L with Pt/Al_2O_3, the increase of the Q_2 concentration results in a decrease of the ammonia conversion. At around 670 K and 50 mol% H_2 or D_2, almost none of the ammonia is decomposed (i.e., DR ≈ 0). At 818 K, the DR also decreases for larger Q_2 concentrations, but the impact is weaker. Similar trends have been obtained for $F^{H,2}$, albeit with a more pronounced impact of the Q_2 partial pressure (discussed below). The same experiments were done for F^L with Ru/Al_2O_3, whose results are given in Fig. 4b). Note that the two temperatures chosen for the ruthenium tests (544 K and 629 K) are lower than those of platinum due to its higher decomposition efficiencies at lower temperatures. Nevertheless, the impact of H_2 and D_2 on the decomposition of NH_3 and ND_3 is less pronounced than with Pt/Al_2O_3 even at lower temperatures, and it is eliminated at 629 K.

The influence of the hydrogen partial pressure on ammonia decomposition with metallic surfaces is a well-understood phenomenon [26]. In general, the so-called inhibition effect due to hydrogen is observed at low temperatures and high hydrogen concentrations. Under these conditions, the hydrogenation of the adsorbed nitrogen occurs at a faster rate than nitrogen desorbs as N_2, which results in a lower decomposition yield. This process is known as Temkin-Pyzhev. On platinum, this process is dependent on the ammonia partial pressure and it was reported to occur from below 650 K, at pressures as low as 0.27 Pa, up to 850 K, at

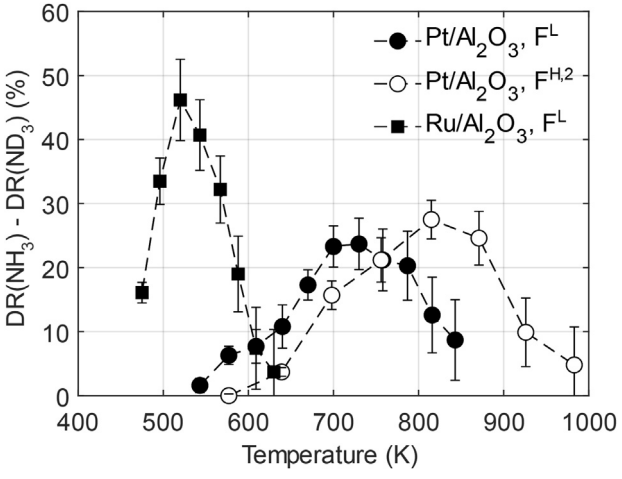

Fig. 3 – Isotopic shift in ammonia decomposition, given by the differences between the DRs of NH_3 and that of ND_3 displayed in Fig. 2 obtained at similar temperatures. Filled squares for Ru/Al_2O_3 with F^L; circles for Pt/Al_2O_3 with F^L (filled) and $F^{H,2}$ (empty).

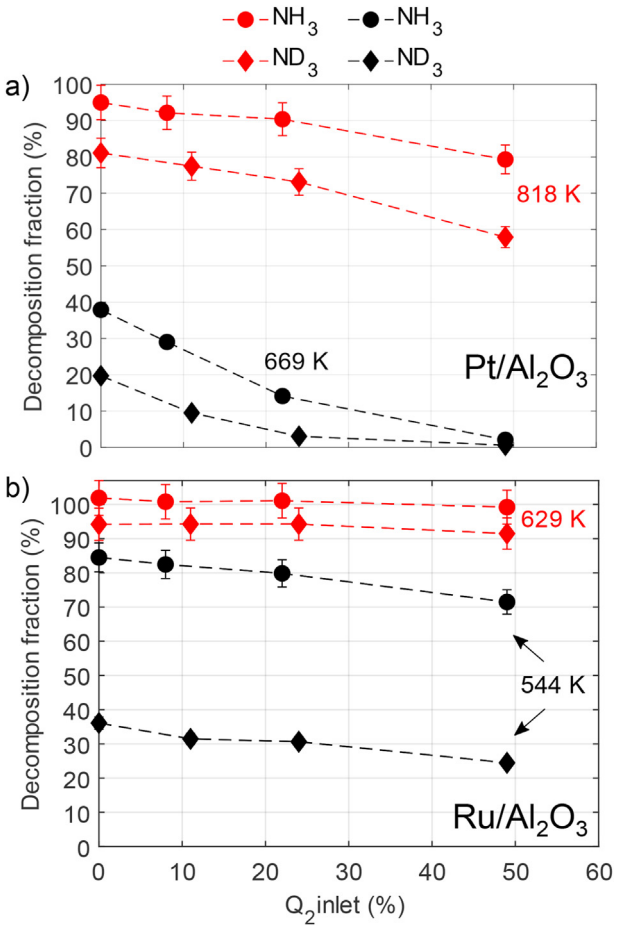

Fig. 4 – Effect of hydrogen content (H_2 or D_2) at the inlet on the decomposition of ammonia (NH_3 or ND_3) using F^L with a) Pt/Al_2O_3 and b) Ru/Al_2O_3. Circles: NH_3, diamonds: ND_3. Red, filled circles: 818 K for a) and 629 K for b); blue, empty circles: 669 K for a) and 544 K for b). (For interpretation of the references to color in this figure legend, the reader is referred to the Web version of this article.)

pressures as high as 80 Pa [27,28]. Chellapa et al. discussed the presence of the inhibition effect for temperatures below 793 K with Ni–Pt/Al_2O_3 up to atmospheric pressure [29]. The results of Fig. 4a), obtained at 1.5 Pa of ammonia partial pressure, are inline with this description, since the inhibition for NH_3 and ND_3 decomposition are observed at 669 and 818 K. The inhibition is also more pronounced at lower temperatures and higher Q_2 concentrations, due to the higher probability of hydrogenation reactions leading to the formation of ammonia. This behaviour was reported as well with ruthenium from pressures as low as 10^{-6} Pa up to atmospheric [25,30]. However, the inhibition effect was observed to depend on the surface sites: on the terrace sites (Ru (1 0 0)) the ammonia decomposition is independent of the hydrogen partial pressure, whereas on the stepped sites (Ru (1 1 10)) the Temkin-Pyzhev mechanism applies [25]. Moreover, the transition between these two processes was reported to occur between 500 and 600 K. Indeed, at 629 K we observe no inhibition effect (Fig. 4b)). At 544 K, a reduction of the ammonia decomposition exists, albeit smaller than that obtained with Pt/Al_2O_3 at higher temperatures. This may be explained by the contribution of both dissociation mechanisms in the transition region and the polycrystallinity of the ruthenium used in our catalyst.

The injection of N_2 up to ≈58 mol% at the same catalyst temperatures did not have a measurable effect on the decomposition of NH_3 and ND_3 for both Pt/and Ru/Al_2O_3 (not shown). These observations are in agreement with other works done for instance with ruthenium-based catalysts [7,30], while with platinum a small N_2 impact has been reported [27].

In order to better compare our results, the degree of inhibition DI, given by Equation (2) and defined such that $DI_{Q_2=0} = 0$, is introduced and plotted in Fig. 5.

$$DI_{Q_2=X} = \frac{DR_{Q_2=0} - DR_{Q_2=X}}{DR_{Q_2=0}} \quad (2)$$

The DIs obtained with Ru/Al_2O_3 are lower than 0.35 for all conditions tested (Fig. 5c and d)). These values contrast to those obtained with Pt/Al_2O_3, for which degrees of inhibition beyond 0.8 were obtained (Fig. 5a and b)), which highlight that the platinum catalyst is more sensitive to the presence of Q_2. On the one side, as previously discussed, the degree of inhibition is found to decrease with the increase of temperature. Since with Ru/Al_2O_3 the DI is approximately 0 at 628 K, then at relevant operating temperatures (673–823 K) the decomposition of both NH_3 and ND_3 should remain unaffected by the presence of Q_2. On the other side, the effect of the temperature in reducing the DI is observed to be generally more important at lower flow-to-mass ratios (Fig. 5a and b)). This is a result of two existing regimes: with low flow-to-mass ratios, the decomposition is more efficient and the increase in temperature translates into a stronger decrease of the DI, i.e. at these conditions the decomposition rate is temperature-limited; with large flow-to-mass ratios, the increase in temperature does not translate into a substantial reduction of the DI, which is compatible to a process limited by the flow-to-mass ratio.

It should be noted that for DIs below 0.10 relatively large uncertainties are obtained, which indicate the limits of accuracy of the experiments at these conditions. For both catalysts, the DI remained approximately zero for all concentrations of N_2 (up to 58 mol%) and temperature range (up to 818 K) used in this work.

Isotopic exchange reactions occurring between NH_3-D_2 and ND_3-H_2

The simultaneous feeding of e.g. DT-ND_3 into the catalyst zone in ITER will unavoidably lead to the formation of heavier ammonia isotopologues through isotopic exchange reactions, which might impact the decomposition of ammonia. The formation of all ammonia isotopologues containing protium and deuterium is discussed in this section.

Due to the large surface areas of the catalysts deployed inside the reactor, isotopic exchange reactions between H_2-D_2, NH_3-D_2 and ND_3-H_2 readily occur even at room temperature. For instance, Fig. 6 displays the formation of HD by simultaneous injection of H_2 and D_2 with Pt/Al_2O_3 using F^L at room temperature. The concentration of HD was fitted with the equation that relates the equilibrium concentration of HD with the equilibration constant $K_{eq}^{HD}(T)$ for the reaction $H_2 + D_2 \rightleftharpoons 2HD$ at a given temperature T (see derivation e.g. here [31]). The resulting fit yielded $K_{eq}^{HD} = 2.47 \pm 19\%$, which is below the expected value (3.26) at this temperature [32]. In Fig. 6, it is also plotted the equilibrium concentration of HD for $K_{eq}^{HD} = 3.26$, which is nevertheless in the range of the estimated uncertainties. One reason for the lower K_{eq}^{HD} might be the low equilibration times. Owing to the one-through characteristic of these experiments, the equilibration times are low and given by the residence time of the inlet flow (on the order of a few seconds). For example, Schlösser et al. carried out similar experiments with equilibration times of ≈25 min achieved through continuous circulation [33].

The experimental run obtained with a 50-50 mol% mixture of ND_3 and H_2 using Pt/Al_2O_3 and $F^{H,2}$, in the range from 575 to 925 K, is shown in Fig. 7. Prior to H_2 introduction, the main peak in the RGA spectra corresponds to that of ND_3, since the decomposition at ≈575 K is fairly low. Due to the decomposition of ND_3 ($m/z = 20$) at the RGA, the other main peak corresponds to ND_2 ($m/z = 18$). Upon H_2 introduction, several peaks suddenly arise as a result of the isotopic exchange reactions occurring on the surface of the metal. The main ammonia isotopologue is NH_2D (note that it has the same mass-to-charge ratio as ND_2, which can be neglected in presence of ND_3-H_2). Equation (3) presents the equilibrium reaction between gaseous H_2 and adsorbed H on the Pt surface, while Equations (4) and (5) present, respectively, ammonia adsorption followed by its decomposition by one D atom. As a result, the available atomic H on the surface can bond to ND_2 to form ND_2H (Equation (6)), while the surface H and D can react to one another, forming HD (Equation (7)) [23]. Upon increasing the catalyst temperature, the concentrations of the ammonia isotopologues decreased as a result of ammonia decomposition. At the same time, the signals of Q_2 (mainly that of HD) and N_2 increased. Interestingly, the relative ratio of the various Q_2 and NQ_3 species was found to weakly depend on the temperature, with typical standard deviations below 10% of the average. At 925 K, H_2 was stopped,

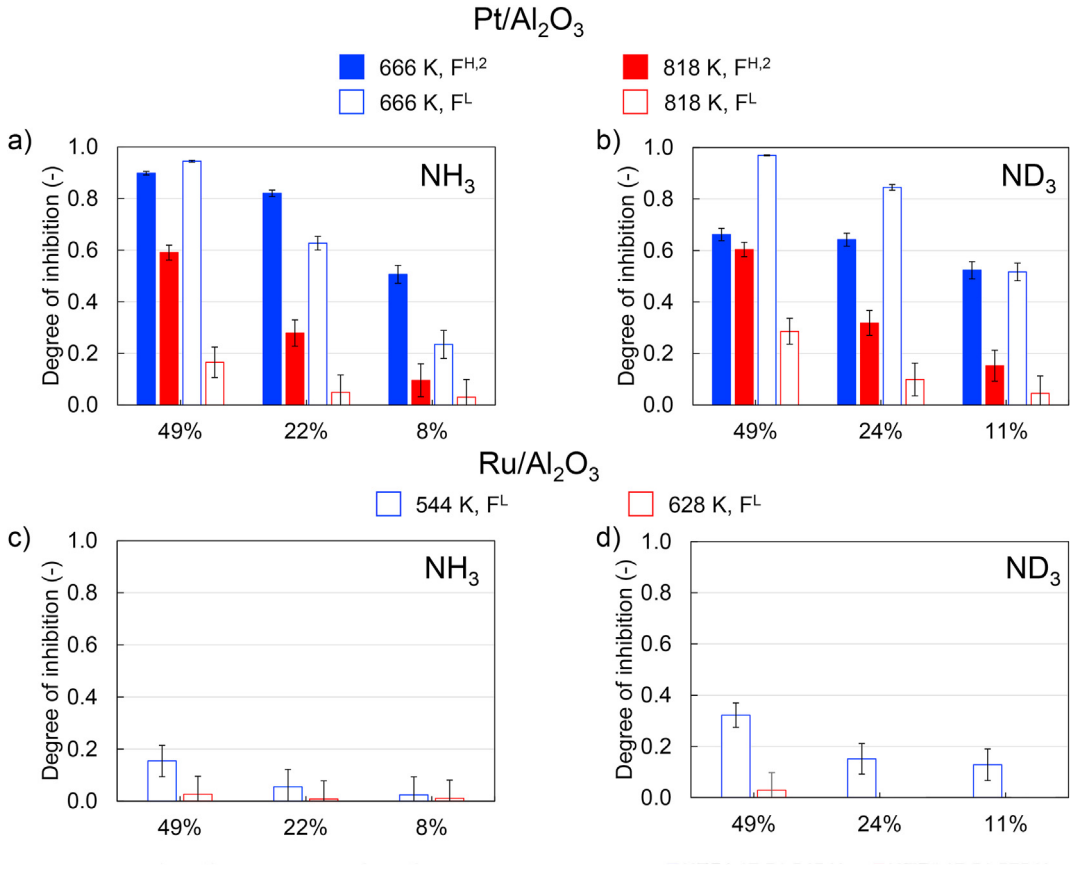

Fig. 5 – Degree of inhibition of ammonia for different concentrations of H_2 (for NH_3, left-hand side plots) and D_2 (for ND_3, right-hand side plots) at the inlet with Pt/Al_2O_3 (top, a) and b)) and Ru/Al_2O_3 (bottom, c) and d)). The empty bars were obtained with F^L, while the filled bars were obtained for with $F^{H,2}$. Red: 818 K (top), 628 K (bottom), blue: 666 K (top), 543 K (bottom). (For interpretation of the references to color in this figure legend, the reader is referred to the Web version of this article.)

which led to an immediate increase of the signals of ND_3, D_2 and N_2. It should be noted that although the signal of ND_3 increased, this does not mean that its decomposition decreased upon H_2 removal. Instead, its signal increased because it became the most important ammonia isotopologue. The increase of N_2 is evidence for an increase in ammonia decomposition upon H_2 removal, which is compatible to the existence of inhibition effect in the mixture ND_3-H_2. These observations are applicable for both catalysts.

$$2H(s) \rightleftharpoons H_2 \quad (3)$$

$$ND_3 \rightarrow ND_3(s) \quad (4)$$

$$ND_3(s) \rightarrow ND_2(s) + D(s) \quad (5)$$

$$ND_2(s) + H(s) \rightarrow ND_2H \quad (6)$$

$$H(s) + D(s) \rightarrow HD \quad (7)$$

Fig. 8 gives the average isotopologue distribution relative to the most important species, NH_2D. For all cases, ND_3 is the compound with the lowest concentration, while NH_3 and ND_2H are found at somewhat similar ratios, with a slightly higher representation of NH_3. Vajo et al. also studied the formation of ammonia isotopologues upon exchange reactions on a platinum wire with equimolar mixtures of NH_3 and D_2 at 0.27 Pa (roughly 10 times lower pressure) [23]. They observed the proportion of 1.00:0.50:0.07 for NH_2D, ND_2H, ND_3, while in this work we obtained: 1.00:0.68:0.37 with F^L and 1.00:0.64:0.26 with $F^{H,2}$. While the values for ND_2H are somewhat in agreement, we observed larger proportions of ND_3.

The inhibition effect of D_2 on NH_3 and H_2 on ND_3 decomposition could also be verified. Fig. 9 compares the decompositions achieved with ammonia alone with that obtained by flowing ammonia along with its symmetric molecular hydrogen isotopologue, using Pt/Al_2O_3 and $F^{H,2}$. A strong suppression of the ammonia decomposition is obtained at low temperatures, in agreement with the results presented previously with 50% Q_2 (Fig. 5). Likewise, the degrees of inhibition for NH_3-D_2 and ND_3-H_2 were very similar to NH_3–H_2 and ND_3-D_2, as shown in Table 2. The same experiments done with Ru/Al_2O_3 and F^L showed a small inhibition effect, even at temperatures below 550 K, in agreement with the results reported for NH_3–H_2 and ND_3-D_2 in Fig. 5. In sum, the effect of Q_2 on the decomposition of NH_3 and ND_3 is the same regardless on whether H_2 or D_2 are used.

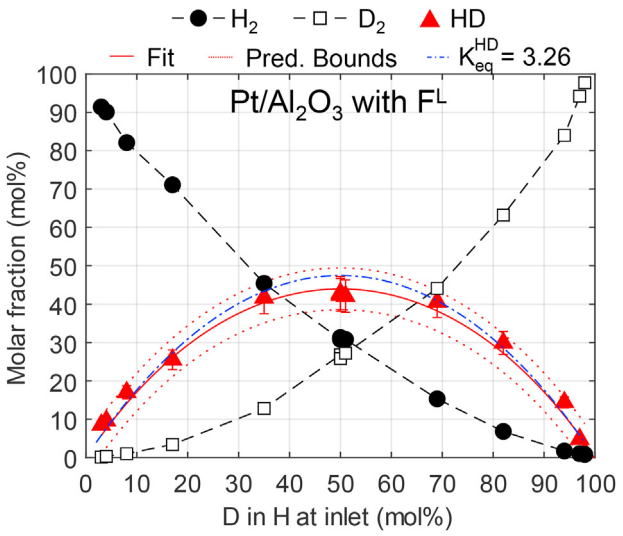

Fig. 6 – Outlet concentrations of H_2, D_2 and HD obtained with Pt/Al_2O_3 using F^L at ≈300 K. The red, pointed line represents the prediction bounds associated with the fit with a confidence interval of 95%. The blue dashed-dot line gives the calculated equilibrium concentration of HD for $K_{eq}^{HD} = 3.26$. (For interpretation of the references to color in this figure legend, the reader is referred to the Web version of this article.)

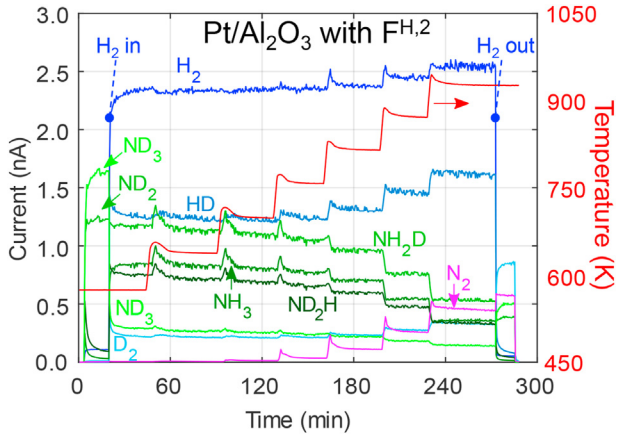

Fig. 7 – Experimental run obtained with an equimolar inlet mixture of ND_3 and H_2 for $F^{H,2}$ with $Pt/-Al_2O_3$ as a function of the catalyst temperature. The NQ_3 isotopologues are shown in green, while the Q_2 molecules are plotted in blue. N_2 is displayed in magenta and the temperature is shown in red (right y-scale). (For interpretation of the references to color in this figure legend, the reader is referred to the Web version of this article.)

Discussion in view of ITER application

The results presented in the previous section aimed at understanding and compare the limitations of the catalysts, which are currently considered for the PMR integrating the TEP of the ITER fusion reactor. However, it is important to point out that in ITER ammonia will be processed using a

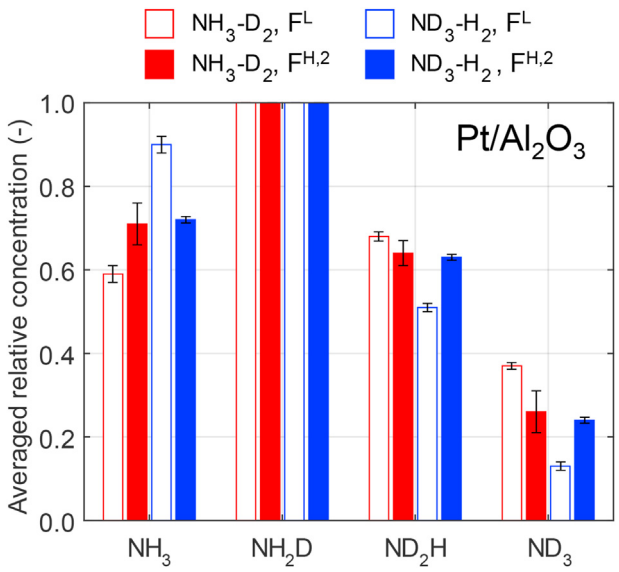

Fig. 8 – Relative concentration of the non-tritiated ammonia isotopologues as a result of isotopic exchange reactions occurring with equimolar mixtures of NH_3-D_2 (red) and ND_3-H_2 (blue) on Pt/Al_2O_3. The values were averaged over the various catalyst temperatures and the uncertainties are the standard deviation of the mean. Empty bars: obtained with F^L, filled bars: with $F^{H,2}$. (For interpretation of the references to color in this figure legend, the reader is referred to the Web version of this article.)

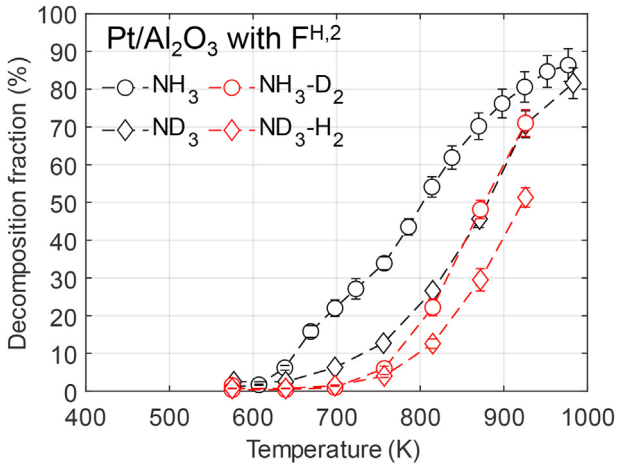

Fig. 9 – Comparison of ammonia decomposition as a function of the catalyst temperature for pure NH_3 and ND_3 (black) and during NH_3-D_2 and ND_3-H_2 isotopic exchange reaction experiments (red). Obtained with Pt/Al_2O_3 and $F^{H,2}$. (For interpretation of the references to color in this figure legend, the reader is referred to the Web version of this article.)

palladium membrane reactor at feed pressures ≈1.013×10^5 Pa. According to the Le Chatelier principle, the decomposition of ammonia is more favourable at lower pressures. However, at the relevant PMR operating temperatures

Table 2 – Degree of inhibition for NQ_3-Q_2 obtained with Pt/Al_2O_3 at around 818 K.

Flow-to-mass ratio	NH_3–H_2	NH_3-D_2	ND_3-D_2	ND_3-H_2
$F^{H,2}$	0.59 ± 0.03	0.58 ± 0.03	0.60 ± 0.03	0.56 ± 0.03
F^{L}	0.17 ± 0.06	0.17 ± 0.06	0.29 ± 0.05	0.19 ± 0.06

(673–823 K), the thermodynamic equilibrium ammonia conversion exceeds 99% even at 1.013×10^5 Pa [34,35]. Thus, its decomposition in the PMR will not be limited by thermodynamics. Moreover, the presence of the palladium (Pd) membrane in the PMR, which is responsible for the removal of the Q_2 species from the feed stream through permeation, favours the increase in ammonia decomposition. Indeed, the simultaneous removal of Q_2 from the feed stream shifts the thermodynamic equilibrium towards the decomposition of ammonia. Several authors have demonstrated the benefit of employing a PMR in respect to a conventional reactor (i.e., a reactor without the Pd membrane) [36–40]. For instance, the recent work of Cechetto et al. makes use of a PMR with a 4.61 μm-thick membrane and 2 wt% Ru/Al_2O_3 [40]. The authors of this work report strong improvements in the decomposition performances of the PMR when compared to the conventional reactor. From 673 to 723 K, the conventional reactor yielded an increase from 65 to 95% of NH_3 decomposition at 4×10^5 Pa. In PMR mode and with 10^5 Pa permeate pressure the conversion of ammonia increased from 70 to 99% in the same temperature range. However, with an evacuated permeate side, the conversion of ammonia remained at 99% for 673–723 K and reaction pressures between 2 and 6×10^5 Pa. The PMR is nevertheless also sensitive to Q_2 inhibition as reported by Collin and Way [41]. No studies have been found on the decomposition of ND_3 using a PMR.

Table 3 compares the performances of the platinum- and ruthenium-based catalysts in the relevant temperature range (673–823 K). Ruthenium exhibited NH_3 and ND_3 decomposition fractions well beyond 90% at temperatures as low as 650 K and no inhibition effect due to Q_2 was detected at 629 K. Moreover, the isotopic effect on the decomposition of NH_3 and ND_3 at these temperatures was observed to be negligible. Thus, even if during ITER operation heavier isotopologues containing tritium will be present, the temperature range at which the PMR will be operated might lead to no isotopic effect on the ammonia decomposition. It should be mentioned that, although an important isotopic effect was observed for Pt/Al_2O_3 in this work, Vajo et al. observed similar decomposition rates of both NH_3 and ND_3 in the range of 27–67 Pa at relevant temperatures [23]. Hence, it is expected that at atmospheric pressure no isotopic effect takes place in presence of Pt/Al_2O_3. The performances of ruthenium for the decomposition of NH_3 were not affected in the range of 0.015–0.058 sccm g^{-1}, but a decrease was observed with 0.200 sccm g^{-1}. This should be of concern in case relatively large amounts of ammonia are released during heating up of the cryotraps. Nevertheless, even with 0.200 sccm g^{-1}, decomposition rates around 90% were achieved at 700 K.

Table 3 – Comparison of the catalysts' performances.

	0.5 wt% Pt/Al_2O_3	0.5 wt% Ru/Al_2O_3
Decomposition rates	–	++
Impact of flow-to-mass ratio	––	–
Isotopic effect	–	+
Inhibition due to Q_2	––	++

In sum, 0.5 wt% Ru/Al_2O_3 is the most suitable catalyst to be employed in the PMR of ITER. Notwithstanding, the selection of the catalyst should be further evaluated in terms of its impact on other decomposition reactions (e.g. water decomposition) foreseen during ITER operation. Studies with an ITER-relevant PMR will start in the near future at the UKAEA laboratories.

Conclusions

The catalytic performances of Pt and Ru on alumina (0.5 wt% loading) for the decomposition of NH_3 and ND_3 have been studied over a wide range of experimental conditions. Decomposition fractions above 80% have been attained only above 750 K with Pt/Al_2O_3, while decompositions above 90% were obtained with Ru/Al_2O_3 already below 700 K. Moreover, the decomposition with Pt/Al_2O_3 was more sensitive to the variation of the flow-to-mass ratio (F_{NH_3}/g-cat) than with Ru/Al_2O_3. For instance, with Pt/Al_2O_3 at 757 K the NH_3 decomposition increases from 34 to 78% with the decrease of F_{NH_3}/g-cat from 0.220 to 0.015 sccm g^{-1}. With $Ru–Al_2O_3$ at 541 K, the same reduction in F_{NH_3}/g-cat led to an increase of the decomposition rate from 49 to 79%. Moreover, the decomposition efficiencies were lower for ND_3 for all conditions tested, thus revealing the existence of isotopic effect. Both catalysts exhibited an inhibition effect due to the simultaneous feeding of ammonia along with hydrogen. However, this effect was significantly more pronounced with Pt/Al_2O_3 at 669 and 818 K. With Ru/Al_2O_3, the inhibition due to hydrogen was suppressed at 629 K. The simultaneous feeding of NH_3-D_2 and ND_3-H_2 revealed the presence of isotopic exchange reactions for all conditions tested. ND_3 was found to be least represented isotopologue, while NH_2D was the most abundant. Upon these exchange reactions, the inhibition on the formation of ammonia was also observed. Our results allow selecting the 0.5 wt% as the catalyst that best meets the requirements for ITER operation. However, the large releases of ammonia during stagewise heating of the cryotraps might also compromise the ammonia decomposition performances if the flows increase to the order of 0.200 sccm g^{-1}.

Declaration of competing interest

The authors declare that they have no known competing financial interests or personal relationships that could have appeared to influence the work reported in this paper.

Acknowledgements

The authors would like to thank the fruitful discussions with Dr. David Demange (ITER Organization) and Richard Knights (UKAEA). This work has been carried out within the framework of the EUROfusion Consortium and has received funding from the Euratom research and training programme 2014-2018 and 2019-2020 under grant agreement no. 633053. The views and opinions expressed herein do not necessarily reflect those of the European Commission. The authors would like to thank the Swiss Federal Office of Energy, the Swiss Nanoscience Institute, the Swiss National Science Foundation and the Federal Office for Education and Science for their Financial support.

REFERENCES

[1] Yin S, Xu B, Zhou X, Au C. A mini-review on ammonia decomposition catalysts for on-site generation of hydrogen for fuel cell applications. Appl Catal Gen 2004;277(1–2):1–9. https://doi.org/10.1016/j.apcata.2004.09.020.

[2] Nasharuddin R, Zhu M, Zhang Z, Zhang D. A technoeconomic analysis of centralised and distributed processes of ammonia dissociation to hydrogen for fuel cell vehicle applications. Int J Hydrogen Energy 2019;44(28):14445–55. https://doi.org/10.1016/j.ijhydene.2019.03.274.

[3] Rathore SS, Biswas S, Fini D, Kulkarni AP, Giddey S. Direct ammonia solid-oxide fuel cells: a review of progress and prospects. Int J Hydrogen Energy 2021;46(71):35365–84. https://doi.org/10.1016/j.ijhydene.2021.08.092.

[4] Lan R, Irvine JT, Tao S. Ammonia and related chemicals as potential indirect hydrogen storage materials. Int J Hydrogen Energy 2012;37(2):1482–94. https://doi.org/10.1016/j.ijhydene.2011.10.004.

[5] Schüth F, Palkovits R, Schlögl R, Su DS. Ammonia as a possible element in an energy infrastructure: catalysts for ammonia decomposition. Energy Environ Sci 2012;5(4):6278–89. https://doi.org/10.1039/C2EE02865D. URL, http://xlink.rsc.org/?DOI=C2EE02865D.

[6] Yin S, Xu B, Zhu W, Ng C, Zhou X, Au C. Carbon nanotubes-supported Ru catalyst for the generation of COx-free hydrogen from ammonia. Catal Today 2004;93–95:27–38. https://doi.org/10.1016/j.cattod.2004.05.011. URL, https://linkinghub.elsevier.com/retrieve/pii/S092058610400207X.

[7] Zheng W, Zhang J, Xu H, Li W. NH3 decomposition kinetics on supported Ru clusters: morphology and particle size effect. Catal Lett 2007;119(3–4):311–8. https://doi.org/10.1007/s10562-007-9237-z. URL, http://link.springer.com/10.1007/s10562-007-9237-z.

[8] Hill AK, Torrente-Murciano L. Low temperature H2 production from ammonia using ruthenium-based catalysts: synergetic effect of promoter and support. Appl Catal B Environ 2015;172–173:129–35. https://doi.org/10.1016/j.apcatb.2015.02.011. URL, https://linkinghub.elsevier.com/retrieve/pii/S0926337315000624.

[9] Levy RB, Boudart M. Platinum-like behavior of tungsten carbide in surface catalysis. Science 1973;181(4099):547–9. https://doi.org/10.1126/science.181.4099.547. URL, https://www.sciencemag.org/lookup/doi/10.1126/science.181.4099.547.

[10] Mukherjee S, Devaguptapu SV, Sviripa A, Lund CR, Wu G. Low-temperature ammonia decomposition catalysts for hydrogen generation. Appl Catal B Environ 2018;226:162–81. https://doi.org/10.1016/j.apcatb.2017.12.039. URL, https://linkinghub.elsevier.com/retrieve/pii/S0926337317311906.

[11] Wood TJ, Makepeace JW, Hunter HMA, Jones MO, David WIF. Isotopic studies of the ammonia decomposition reaction mediated by sodium amide. Phys Chem Chem Phys 2015;17(35):22999–3006. https://doi.org/10.1039/C5CP03560K. URL, http://xlink.rsc.org/?DOI=C5CP03560K.

[12] Glugla M, Lässer R, Dörr L, Murdoch D, Haange R, Yoshida H. The inner deuterium/tritium fuel cycle of ITER. Fusion Eng Des 2003;69(1–4):39–43. https://doi.org/10.1016/s0920-3796(03)00231-x.

[13] Kallenbach A, Bernert M, Dux R, Casali L, Eich T, Giannone L, Herrmann A, McDermott R, Mlynek A, Müller HW, Reimold F, Schweinzer J, Sertoli M, Tardini G, Treutterer W, Viezzer E, Wenninger R, Wischmeier M. The ASDEX Upgrade Team, Impurity seeding for tokamak power exhaust: from present devices via ITER to DEMO. Plasma Phys Contr Fusion 2013;55(12):124041. https://doi.org/10.1088/0741-3335/55/12/124041. URL, https://iopscience.iop.org/article/10.1088/0741-3335/55/12/124041.

[14] de Castro A, Alegre D, Tabarés F. Ammonia formation in N2/H2 plasmas on ITER-relevant plasma facing materials: surface temperature and N2 plasma content effects. J Nucl Mater 2015;463:676–9. https://doi.org/10.1016/j.jnucmat.2014.12.038. URL, https://linkinghub.elsevier.com/retrieve/pii/S0022311514009805.

[15] Laguardia L, Caniello R, Cremona A, Dellasega D, Dell'Era F, Ghezzi F, Gittini G, Granucci G, Mellera V, Minelli D, Pallotta F, Passoni M, Ricci D, Vassallo E. Ammonia formation and W coatings interaction with deuterium/nitrogen plasmas in the linear device GyM. J Nucl Mater 2015;463:680–3. https://doi.org/10.1016/j.jnucmat.2014.12.087. URL, https://linkinghub.elsevier.com/retrieve/pii/S0022311514010307.

[16] Ben Yaala M, Saeedi A, Scherrer D-F, Moser L, Steiner R, Zutter M, Oberkofler M, De Temmerman G, Marot L, Meyer E. Plasma-assisted catalytic formation of ammonia in N_2–H_2 plasma on a tungsten surface. Phys Chem Chem Phys 2019;21(30):16623–33. https://doi.org/10.1039/C9CP01139K. URL, http://xlink.rsc.org/?DOI=C9CP01139K.

[17] Antunes R, Steiner R, Romero Muñiz C, Soni K, Marot L, Meyer E. Plasma-Assisted catalysis of ammonia using tungsten at low pressures: a parametric study. ACS Appl Energy Mater 2021;4(5):4385–94. https://doi.org/10.1021/acsaem.0c03217. URL, https://pubs.acs.org/doi/10.1021/acsaem.0c03217.

[18] Wilson J, Becnel J, Demange D, Rogers B. The ITER tokamak exhaust processing system design and substantiation. Fusion Sci Technol 2019;75(8):794–801. https://doi.org/10.1080/15361055.2019.1642089. URL, https://www.tandfonline.com/doi/full/10.1080/15361055.2019.1642089.

[19] Knights R, Benayas J, Sabin K, Ng S, Wohlers A, Tijssen T, Demange D, Willms S, Brennan D. Initial testing of an inside-out type palladium membrane reactor for recovery of hydrogen from hydrocarbons or water. Fusion Eng Des 2021;168:112641. https://doi.org/10.1016/j.fusengdes.2021.112641.

[20] Iost KN, Borisov VA, Smirnova NS, Temerev VL, Surovikin YV, Shlyapin DA, Tsyrulnikov PG. Resistance for methanation and activity in ammonia decomposition catalysts Ru-Rb/Subunit, Omsk, Russia. 2019. p. 20033. https://doi.org/10.1063/1.5122932. URL, http://aip.scitation.org/doi/abs/10.1063/1.5122932.

[21] Makepeace JW, Wood TJ, Hunter HMA, Jones MO, David WIF. Ammonia decomposition catalysis using non-stoichiometric lithium imide. Chem Sci 2015;6(7):3805–15. https://doi.org/10.1039/C5SC00205B. URL, http://xlink.rsc.org/?DOI=C5SC00205B.

[22] Wood TJ, Makepeace JW, David WIF. Isotopic studies of the ammonia decomposition reaction using lithium imide catalyst. Phys Chem Chem Phys 2017;19(6):4719–24. https://doi.org/10.1039/C6CP07734J. URL, http://xlink.rsc.org/?DOI=C6CP07734J.

[23] Vajo JJ, Tsai W, Weinberg WH. Mechanistic details of the heterogeneous decomposition of ammonia on platinum. J Phys Chem 1985;89(15):3243–51. https://doi.org/10.1021/j100261a017. URL, https://pubs.acs.org/doi/abs/10.1021/j100261a017.

[24] Boisen A, Dahl S, Norskov J, Christensen C. Why the optimal ammonia synthesis catalyst is not the optimal ammonia decomposition catalyst. J Catal 2005;230(2):309–12. https://doi.org/10.1016/j.jcat.2004.12.013. URL, https://linkinghub.elsevier.com/retrieve/pii/S0021951704006013.

[25] Egawa C, Nishida T, Naito S, Tamaru K. Ammonia decomposition on (1 1 10) and (0 0 1) surfaces of ruthenium. J Chem Soc, Faraday Trans 1: Physical Chemistry in Condensed Phases 1984;80(6):1595. https://doi.org/10.1039/f19848001595.

[26] Tamaru K. A "new" general mechanism of ammonia synthesis and decomposition on transition metals. Acc Chem Res 1988;21(2):88–94. https://doi.org/10.1021/ar00146a007. URL, https://pubs.acs.org/doi/abs/10.1021/ar00146a007.

[27] Loffler D. Kinetics of NH3 decomposition on polycrystalline Pt. J Catal 1976;41(3):440–54. https://doi.org/10.1016/0021-9517(76)90245-1. URL, https://linkinghub.elsevier.com/retrieve/pii/0021951776902451.

[28] Tsai W, Vajo JJ, Weinberg WH. Inhibition by hydrogen of the heterogeneous decomposition of ammonia on platinum. J Phys Chem 1985;89(23):4926–32. https://doi.org/10.1021/j100269a009.

[29] Chellappa A, Fischer C, Thomson W. Ammonia decomposition kinetics over ni-pt/al2o3 for PEM fuel cell applications. Appl Catal Gen 2002;227(1–2):231–40. https://doi.org/10.1016/s0926-860x(01)00941-3.

[30] Prasad V, Karim AM, Arya A, Vlachos DG. Assessment of overall rate expressions and multiscale, microkinetic model uniqueness via experimental data injection: ammonia decomposition on Ru/γ-Al_2O_3 for hydrogen production. Ind Eng Chem Res 2009;48(11):5255–65. https://doi.org/10.1021/ie900144x. URL, https://pubs.acs.org/doi/10.1021/ie900144x.

[31] Antunes R. Experimental and numerical study on MFI-ZSM-5 zeolite membranes for tritium separation and recovery in nuclear fusion reactors. Ph.D. thesis. University of Lisbon; 2019. URL, http://hdl.handle.net/10451/42331.

[32] Pyper JW, Kelly EM, Magistad JG, Tsugawa RT, Roberts PE, Souers PC. Quadrupole mass-filter sensitivities of H_2, HD, D_2 and T_2, and the kinetics of β-particle induced exchange between H2, D2 and T2 at 25.4 °c. Lawrence Livermore Laboratory 1978. Tech. rep. https://www.osti.gov/servlets/purl/5043666.

[33] Schlösser M, Seitz H, Rupp S, Herwig P, Alecu CG, Sturm M, Bornschein B. In-line calibration of Raman systems for analysis of gas mixtures of hydrogen isotopologues with sub-percent accuracy. Anal Chem 2013;85(5):2739–45. https://doi.org/10.1021/ac3032433.

[34] Slycke J, Mittemeijer E, Somers M. Thermodynamics and kinetics of gas and gas–solid reactions. In: Thermochemical surface engineering of steels. Elsevier; 2015. p. 3–111. https://doi.org/10.1533/9780857096524.1.3.

[35] Ojelade OA, Zaman SF. Ammonia decomposition for hydrogen production: a thermodynamic study. Chem Pap 2020;75(1):57–65. https://doi.org/10.1007/s11696-020-01278-z.

[36] Collins JP. Catalytic decomposition of ammonia in a membrane reactor. PhD thesis. Oregon State University; 1993. URL, http://hdl.handle.net/1957/19338.

[37] García-García F, Ma YH, Rodríguez-Ramos I, Guerrero-Ruiz A. High purity hydrogen production by low temperature catalytic ammonia decomposition in a multifunctional membrane reactor. Catal Commun 2008;9(3):482–6. https://doi.org/10.1016/j.catcom.2007.07.036. URL, https://linkinghub.elsevier.com/retrieve/pii/S1566736707003299.

[38] Itoh N, Oshima A, Suga E, Sato T. Kinetic enhancement of ammonia decomposition as a chemical hydrogen carrier in palladium membrane reactor. Catal Today 2014;236:70–6. https://doi.org/10.1016/j.cattod.2014.02.054. URL, https://linkinghub.elsevier.com/retrieve/pii/S0920586114002375.

[39] Liu J, Ju X, Tang C, Liu L, Li H, Chen P. High performance stainless-steel supported Pd membranes with a finger-like and gap structure and its application in NH3 decomposition membrane reactor. Chem Eng J 2020;388:124245. https://doi.org/10.1016/j.cej.2020.124245. URL, https://linkinghub.elsevier.com/retrieve/pii/S1385894720302369.

[40] Cechetto V, Di Felice L, Medrano JA, Makhloufi C, Zuniga J, Gallucci F. H2 production via ammonia decomposition in a catalytic membrane reactor. Fuel Process Technol 2021;216:106772. https://doi.org/10.1016/j.fuproc.2021.106772. URL, https://linkinghub.elsevier.com/retrieve/pii/S0378382021000515.

[41] Collins JP, Way J. Catalytic decomposition of ammonia in a membrane reactor. J Membr Sci 1994;96(3):259–74. https://doi.org/10.1016/0376-7388(94)00138-3. URL, https://linkinghub.elsevier.com/retrieve/pii/0376738894001383.